**Title: Direct binding of a fungal effector by the wheat RWT4 tandem kinase activates defense**

**Authors:**

Yi-Chang Sung[1], Yinghui Li[1, 2, 3], Zoe Bernasconi[4], Suji Baik[1], Soichiro Asuke[5], Beat Keller[4], Tzion Fahima[2], Gitta Coaker[1*]

Author Affiliations:

[1]Department of Plant Pathology, University of California, Davis, CA, U.S.A.

[2]Institute of Evolution and the Department of Evolutionary and Environmental Biology, University of Haifa, 199 Abba-Hushi Avenue, Mt. Carmel, 3498838 Haifa, Israel

[3]Triticeae Research Institute, Sichuan Agricultural University, Chengdu 611130, Sichuan, China

[4]Department of Plant and Microbial Biology, University of Zurich, Zollikerstrasse 107, 8008 Zurich, Switzerland

[5]Graduate School of Agricultural Science, Kobe University, Kobe 657-8501, Japan

* Corresponding author: G. Coaker, glcoaker@ucdavis.edu

**Abstract**

Plants have intricate innate immune receptors that detect pathogens. Research has intensely focused on two receptor classes recognizing external and internal threats. Recent research has identified a class of disease resistance proteins called tandem kinase proteins (TKPs). We investigated RWT4, a wheat TKP that confers resistance to the devastating fungal pathogen *Magnaporthe oryzae*. We established a rice protoplast system, revealing RWT4 specifically recognizes the AvrPWT4 effector, leading to the transcription of defense genes and inducing cell death. RWT4 possesses both kinase and pseudokinase domains, with its kinase activity essential for defense. RWT4 directly interacts with and transphosphorylates AvrPWT4. Biolayer interferometry revealed both RWT4 kinase and pseudokinase regions bind the effector. Sequence similarity and structural modeling revealed an integrated partial kinase duplication in RWT4's kinase region as critical for effector interaction and defense activation. Collectively, these findings demonstrate that TKPs can directly bind a recognized effector, leading to downstream defense activation.

31 **Introduction**

32 Plant genomes encode multiple innate immune receptors capable of recognizing diverse
33 pathogen classes [1]. These immune receptors recognize pathogen features such as conserved
34 molecular patterns or specialized secreted pathogen effector proteins [1]. The main classes of plant
35 immune receptors are broadly categorized into cell-surface localized receptors, including
36 receptor-like kinases (RLKs) or receptor-like proteins (RLPs), as well as intracellular nucleotide-
37 binding domain leucine-rich repeat (NLR) immune receptors [2,3]. Most identified and well-studied
38 receptors belong to RLKs/RLPs or NLRs, also known as canonical resistance genes [4]. Recently,
39 kinase fusion proteins (KFP) have emerged as new players in plant immunity. KFPs contain distinct
40 protein architecture, including dual-kinase domains termed tandem kinase proteins (TKPs) or
41 kinase fused with an integrated domain [5].

42

43 To date, more than 100 TKPs have been found across plant species, spanning both dicots and
44 monocots [6,7]. A more recent TKP atlas comprising 104 angiosperm genomes identified 2,682 TKPs
45 [8]. TKPs represent a protein, not a gene, family since their kinase domains can be derived from
46 different kinase (sub)families [9]. However, TKPs conferring disease resistance have been exclusively
47 identified from the *Triticeae* tribe. Currently, ten *Triticeae* TKPs have been identified that confer
48 resistance to biotrophic or hemibiotrophic fungal pathogens [5,9,10]. Barley RPG1 conferring
49 resistance to barley stem rust was the first TKP identified [11]. Subsequent cloning of wheat
50 resistance proteins, WTK1 to WTK7-TM and RWT4, also revealed dual-kinase architecture [6,10,12-
51 15]. KFPs can also contain integrated non-kinase domains. For example, Sr43 (kinase-DUF347-
52 DUF668) and WTK6-vWA (TKP-vWA), have been cloned with resistance to stem rust and leaf rust,
53 respectively [16,17]. NLR immune receptors can also carry integrated domains responsible for
54 directly binding recognized pathogen effectors, leading to defense activation and cell death [18].
55 However, it is unclear if TKPs can directly recognize pathogen effectors or other pathogen
56 components.

57

58 Current data, primarily from mutant analyses, indicates that both domains are required for TKP-
59 mediated resistance, which includes eliciting plant cell death. Wheat Tandem Kinase 1 (WTK1),

60 conferring resistance to yellow rust, induces rapid and localized cell death post-haustoria
61 formation, suggesting that defense activation requires the perception of an unknown effector [9].
62 Mutagenesis assays have revealed the requirement of both kinase and pseudokinase domains for
63 WTK1 function [9]. Similarly, mutants in RPG1's kinase or pseudokinase domain exhibited full
64 susceptibility to *Puccinia graminis* f. sp. *tritici* [19]. RPG1 exhibits *in vitro* autophosphorylation
65 activity, is rapidly phosphorylated upon exposure to avirulent spores, and can also induce cell
66 death [19,20]. These data indicate that TKPs are rapidly activated upon pathogen perception and can
67 elicit hallmarks of innate immune responses, including cell death [6,10,14,21,22].
68
69 Recently, the *Rwt4* TKP was cloned from the D-genome of hexaploid wheat [15]. RWT4 recognizes
70 the PWT4 effector from *Magnaporthe oryzae* (syn *Pyricularia oryzae*) pathotype *Avena*, leading
71 to an incompatible interaction [23]. *M. oryzae* is composed of host-specific subgroups that can cause
72 disease in rice, finger millet, oat, perennial ryegrass, and wheat. *M. oryzae* poses a threat to global
73 wheat production [24]. The *M. oryzae* host jump to wheat required loss of pathogen recognition by
74 the TKP *Rwt4* and the NLR *Rwt3* [15].
75
76 Here, we examined RWT4 as a model for TKP activation. We demonstrate that RWT4 directly
77 binds and phosphorylates the recognized effector AvrPWT4, but not an unrecognized VirPWT4
78 allele. Furthermore, RWT4 can be transferred to a rice protoplast system and confer defense
79 activation in the presence of AvrPWT4. Structure-function analyses identified key RWT4 residues
80 required for effector binding and defense activation. These findings provide detailed mechanistic
81 insights into TKP effector binding and activation.
82
83 **Results**
84 ***RWT4 recognizes AvrPWT4 in wheat and rice***
85 *Rwt4* is located in the D genome of hexaploid wheat [15]. First, we phenotyped the hexaploid wheat
86 cultivars Norin 4 (*Rwt4*), Cadenza (*Rwt4*), Hope (*rwt4*), and Chinese Spring (*rwt4*) for their
87 responses to inoculation with spores of *M. oryzae* pathotype *Triticum* (MoT) isolate Br48 and its
88 *AvrPwt4* transformants. Disease symptoms were recorded four days post-inoculation (dpi).

89 Leaves infected with Br48 showed moderate to severe symptoms across all tested samples. As
90 expected, the Br48 transformant carrying *AvrPwt4* failed to cause comparable symptoms in Norin
91 4 and Cadenza, demonstrating that lines harboring *Rwt4* are resistant to *AvrPwt4*-carrying strains
92 (Fig. 1a, Table S1). All genotypes we tested lack *Rmg8*, an MCTP-kinase that recognizes another
93 *M. oryzae* effector [25,26].
94
95 Next, we sought to identify a rapid plant system to investigate TKP activation. We employed a rice
96 protoplast system to transiently co-express *Rwt4* and *Pwt4* and assayed defense responses,
97 including cell death and defense gene expression (Fig. 1b). Luminance-based cell viability assays
98 were conducted to evaluate the ability of *Rwt4* to specifically recognize *AvrPwt4* when expressed
99 in rice. Protoplasts co-expressing *AvrPwt4* and the resistant Cadenza allele of *Rwt4* ($Rwt4^{Ca}$)
100 exhibited a significant reduction in viability compared to cells transfected with $Rwt4^{Ca}$ plus an
101 empty vector (Fig. 1c, $p<0.0001$). In contrast, co-transfecting the susceptible Chinese Spring allele
102 of *Rwt4* ($Rwt4^{Cs}$) and *AvrPwt4* failed to cause cell death (Fig. 1c). Furthermore, we examined
103 RWT4's specificity in recognizing PWT4 for defense activation by co-transfecting $Rwt4^{Ca}$ with
104 either *AvrPwt4* or *VirPwt4* in rice protoplasts. A significant strong reduction of cell viability was
105 specifically observed in cells co-transfected with $Rwt4^{Ca}$ and *AvrPwt4* but not in cells co-
106 transfected with either *VirPwt4* or an empty vector (Fig. 1d, $p<0.0001$). Similarly, we measured
107 defense gene activation and observed that the defense marker genes *RSOsPR10*, *OsPr10a* and
108 *OsRin4* [27-29] were specifically induced in cells co-transfected with $Rwt4^{Ca}$ and *AvrPwt4* (Fig. 1e).
109 RWT4 and PWT4 effectors were detectable in rice protoplasts by western blot (Fig. S1). These
110 results demonstrate that RWT4 is functional when transferred to rice and can specifically
111 recognize the AvrPWT4 effector.
112
113 ***The kinase activity of RWT4 is required for defense activation***
114 *Rwt4* was identified as a tandem kinase encoding a kinase-pseudokinase domain organization. To
115 explore the kinase domain family/subfamily of $RWT4^{Ca}$, we conducted a sequence homology
116 search for the $RWT4^{Ca}$ kinase domain (amino acids 189-470) and pseudokinase domain (amino
117 acids 554-840) in The Arabidopsis Information Resource (TAIR, www.arabidopsis.org), identifying

118 AT4G00960 and AT4G05200 as kinase and pseudokinase orthologs, respectively. Analysis of their
119 kinase family/subfamily using the annotated Arabidopsis kinome dataset [30] revealed that both of
120 the domains belong to the LRR_8B kinase subfamily, predominantly associated with cysteine-rich
121 receptor-like kinases for defense regulation. The two regions are interconnected by a linker region,
122 which is flexible and intrinsically disordered (Fig. 2a). Except for WTK1, all other identified TKPs
123 controlling disease resistance contain LRR_8B kinase domains [9,10,16].
124
125 We explored the importance of kinase activity in RWT4-mediated defense. We expressed and
126 purified recombinant RWT4 proteins including full length wild type RWT4$^{Ca}$ (His-MBP-RWT4$^{Ca}$), its
127 kinase region (His-MBP-K), pseudokinase region (His-MBP-PK), and a kinase-dead variant (His-
128 MBP-RWT4$^{Ca_K217R/K327R}$), with mutations in the two conserved lysines located within the ATP
129 binding motif (K217R) and the catalytic residue (K327R) predicted via InterPro [31,32] (Fig. 2b).
130 Immunoblot analysis employing a phosphor-Thr/Tyr antibody detected phosphorylated His-MBP-
131 RWT4$^{Ca}$ and His-MBP-K while the signal was removed by treatment with lambda protein
132 phosphatase (Fig. 2c), suggesting RWT4$^{Ca}$ and His-MBP-K are capable of autophosphorylation. In
133 contrast, RWT4's pseudokinase region and MBP-RWT4$^{Ca_K217R/K327R}$ exhibited no detectable
134 phosphorylation by western blot (Fig. 2c). Subsequent kinase assays using [$^{32}$P]γATP detected *de*
135 *novo* phosphorylation of His-MBP-RWT4$^{Ca}$ and His-MBP-K, whereas His-MBP-PK and His-MBP-
136 RWT4$^{Ca_K217R/K327R}$ failed to exhibit kinase activity (Fig. 2d). Western blot with anti-HIS and
137 Coomassie-stained SDS-PAGE analysis further revealed a size shift between His-MBP-RWT4$^{Ca}$ and
138 His-MBP-RWT4$^{Ca_K217R/K327R}$ (Fig. 2b and 2c), further confirming that RWT4$^{Ca_K217R/K327R}$ serves as a
139 kinase dead variant of RWT4$^{Ca}$. These data demonstrate that RWT4 is an active kinase and
140 contains kinase-pseudokinase architecture.
141
142 Next, we employed mass spectrometry to identify unique RWT4 phosphorylation sites upon
143 incubation with AvrPWT4 *in vitro*. RWT4 was phosphorylated at multiple sites in the absence of
144 AvrPWT4. Four unique phosphorylated residues were identified only after incubation with
145 recombinant AvrPWT4, two located within the kinase and two within the pseudokinase (Fig. S2,
146 S3). One of these phosphorylated residues, Y204, resides within the ATP binding motif (195-217

147 amino acids), just proximal to the glycine-rich loop of RWT4's kinase domain (KD) and is a
148 conserved residue in the kinase of other TKP LRR_8B members (Fig. S3). The remaining three
149 residues, T164, S609, S803, are not conserved across the kinase/pseudokinase of other TKP
150 LRR_8B members.
151
152 To determine if RWT4's kinase activity is required for defense induction, we co-transfected
153 *AvrPwt4* with either *Rwt4*$^{Ca}$ or *Rwt4*$^{Ca_K217R/K327R}$ and measured cell viability as an indicator of
154 defense activation. Unlike wild type *Rwt4*$^{Ca}$, which strongly reduced cell viability when recognizing
155 *AvrPwt4*, cells co-transfected with *AvrPwt4* and *Rwt4*$^{Ca_K217R/K327R}$ exhibited no significant
156 decrease in cell viability (Fig. 2e, $p<0.0001$). Western blot detected protein equal expression of
157 RWT4$^{Ca}$ and RWT4$^{Ca_K217R/K327R}$ in rice protoplasts (Fig. S1a). These data collectively demonstrate
158 that RWT4 kinase activity is necessary for defense responses mediated by perception of AvrPWT4.
159
160 ***RWT4 phosphorylates AvrPWT4, but not the unrecognized effector VirPWT4***
161 Next, we sought to investigate whether RWT4 phosphorylates AvrPWT4. Purified recombinant
162 His-MBP-RWT4$^{Ca}$ was mixed with GST-AvrPWT4 or GST-VirPWT4 at 1:1 molar ratio 30 min prior to
163 the kinase assay using [$^{32}$P]γATP. The common kinase substrate myelin basic protein (MyBP) was
164 included as a positive control. Phosphorylated GST-AvrPWT4 was detected from samples
165 incubated with His-MBP-RWT4$^{Ca}$ (Fig. 2f) or His-MBP-K (Fig. S4a). However, no phosphorylated
166 GST-AvrPWT4 was observed from samples incubated with His-MBP-PK (Fig. S4a) or the kinase
167 dead variant His-MBP-RWT4$^{Ca_K217R/K327R}$ (Fig. S4b). Furthermore, RWT4$^{Ca}$ did not phosphorylate
168 GST-VirPWT4 when using recombinant proteins (Fig. 2f). These findings demonstrate that RWT4$^{Ca}$
169 specifically transphosphorylates the recognized effector AvrPWT4 *in vitro*.
170
171 To further investigate the biological significance of AvrPWT4 phosphorylation, we mapped
172 AvrPWT4 phosphorylation sites by mass-spectrometry and identified five phosphorylated
173 residues (Fig. S5a). Comparison of recognized and unrecognized alleles of PWT4 revealed that the
174 T45 residue is unique to AvrPWT4 but absent in VirPWT4 (Fig. S5b, Fig. 2g). We generated the
175 phosphorylation null mutant *AvrPwt4*$^{T45A}$ and tested its ability to be recognized by RWT4$^{Ca}$ in rice

176 protoplasts. However, *AvrPwt4*$^{T45A}$ had a similar ability to induce cell death in protoplasts as wild-
177 type *AvrPwt4* when co-transfected with *Rwt4*$^{Ca}$, suggesting the effector phosphorylation at this
178 residue is not required for RWT4-mediated defense (Fig. 2g, $p<0.0001$). Western blot detected
179 AvrPWT4 and AvrPWT4$^{T45A}$ expression from protoplasts (Fig. S5c).
180
181 ***RWT4$^{Ca}$ directly and specifically interacts with AvrPWT4***
182 It has been an unsolved question if TKPs can act as a receptor for a corresponding effector. Yeast
183 two-hybrid demonstrated an interaction between RWT4$^{Ca}$ and AvrPWT4 but no interaction with
184 VirPWT4 (Fig. 3a). Western blot analysis confirmed the protein expression of RWT4$^{Ca}$, AvrPWT4,
185 and VirPWT4 in yeast (Fig. S6). To further validate that the RWT4 TKP can directly interact with
186 AvrPWT4, we utilized Bio-layer interferometry (BLI) to characterize binding kinetics. RWT4$^{Ca}$ was
187 purified with a His-tag for immobilizing to the biosensors, while AvrPWT4 and VirPWT4 were
188 expressed with a GST tag which was subsequently removed by TEV protease treatment during
189 purification (Fig. 3b). Based on the molecular weight and yields of purified proteins, a 1.5x dilution
190 of molar concentration gradient of effectors were prepared from 10 µM to 51 nM as ligands, while
191 purified His-RWT4$^{Ca}$ was immobilized to the Octet NTA biosensors as analytes. Strong binding
192 kinetics between RWT4$^{Ca}$ were observed for all tested concentrations of AvrPWT4 showing
193 wavelength shifts from 0.6844 nm to 0.0264 nm, with binding constants ($K_D$) less than $1x10^{-12}$ (Fig.
194 3c and Table S2). In contrast, the binding affinity of RWT4$^{Ca}$ to VirPWT4 is weak and unstable,
195 showing wavelength shifts from 0.1754 nm to 0.0023 nm with a $K_D$ value greater than $10^{-7}$ (Fig.
196 3c and Table S2). Background binding to GST exhibited similar weak kinetics comparable to the
197 binding observed between His-RWT4$^{Ca}$ and VirPWT4 (Fig. 3c and Table S2). These results
198 demonstrate that RWT4$^{Ca}$ has direct, stable, and specific binding to AvrPWT4.
199
200 Further BLI assays were conducted to determine which RWT4 $^{Ca}$ domain is required for AvrPWT4
201 interaction. Due to challenges in obtaining high-quality proteins of kinase and pseudokinase with
202 a His-tag, we expressed proteins with a His-MBP tag to promote solubility. Interestingly, both His-
203 MBP-K and His-MBP-PK demonstrated measurable binding to AvrPWT4 within concentrations
204 ranging from 10 µM to 173 nM, exhibiting similar binding constants although His-MBP-PK

205 displayed weaker wavelength shifts (Fig. 3d and Table S3). Notably, the full-length His-MBP-
206 RWT4$^{Ca}$ exhibited stronger binding affinity than its individual domains, and all three tested
207 proteins showed no binding to GST (Fig. 3d and Table S3).
208
209 To validate the association between RWT4$^{Ca}$ and AvrPWT4, we performed co-
210 immunoprecipitation assays in *Nicotiana benthamiana*. AvrPWT4-GFP or VirPWT4-GFP were co-
211 expressed with RWT4$^{Ca}$-3xFLAG or an empty vector (EV-3xFLAG). Immunoblotting results
212 demonstrated that AvrPWT4-GFP strongly associated with RWT4$^{Ca}$-3xFLAG, while no detectable
213 interaction between VirPWT4-GFP and RWT4$^{Ca}$-3xFLAG was observed (Fig. 3e). RWT4$^{Ca}$-3xFLAG,
214 AvrPWT4-GFP, and VirPWT4-GFP were expressed and detected by immunoblotting in *N.*
215 *benthamiana* (Fig. 3e). Collectively, these *in vitro* and *in vivo* results indicate that RWT4 functions
216 as a receptor for AvrPWT4, with both kinase and pseudokinase involved in effector binding.
217
218 ***Structure-guided identification of RWT4 specificity***
219 We further investigated the sequence or structural features determining the binding of RWT4 to
220 AvrPWT4. Through pairwise sequence alignment, the N-terminus of RWT4 (amino acids 1-142)
221 was found to exhibit similarity to another section (amino acids 150-290) comprising part of the
222 kinase domain. InterPro annotations identified a partial kinase (amino acids 25-145) within the
223 segment. Subsequent sequence alignment between this partial kinase and RWT4' kinase domain
224 identified amino acids 39-142 that exhibited 63.83% sequence similarity to a fragment of the
225 kinase domain (amino acids 150-290) (Fig. 4a). This conserved region exhibits both DNA and
226 protein sequence similarity to the KD and thus termed an integrated kinase duplication (KDup)
227 (Fig. 4a and 4b). KDup contains a portion of a kinase ATP-binding motif but the predicted active
228 site K217 is not included. By employing AlphaFold2, the structure model of RWT4$^{Ca}$ revealed that
229 the KDup (yellow) comprises a short $\alpha$-helix and a $\beta$-sheet, resembling the N-terminus of the
230 kinase domain (green) (Fig. 4c and Fig. S7a). These observations demonstrate RWT4$^{Ca}$ contains
231 an integrated partial kinase duplication, KDup.
232

233 Next, we predicted the RWT4$^{Ca}$-AvrPWT4 protein complex through AlphaFold-Multimer [33] (Fig.
234 5a, left and Fig. S7). Structural modeling suggests that AvrPWT4 (purple) mediates interactions
235 between the KDup (yellow) and pseudokinase (blue). We identified potential binding regions in
236 the KDup (117-127), the KD (261-270) and two regions in the PKD (551-560, 627-645). Next, we
237 compared *Rwt4* alleles from known *MoT*-resistant wheat cultivars (Norin 4, Cadenza, Jagger,
238 Paragon and Claire) with susceptible cultivars (Chinese Spring and CDC Stanley) [15,23] (Fig. S8 and
239 Table S4). We identified sequence polymorphisms within the predicted KDup binding region (117-
240 127) and PKD region 2 (627-645) (Fig. 5b). Additionally, a six-amino-acid extension at the C-
241 terminus was specifically conserved in susceptible *Rwt4* alleles (Fig. 5b).
242
243 To test the importance of the identified binding regions from AlphaFold-Multimer and sequence
244 analyses, we generated RWT4 variants by replacing sequences between resistant and susceptible
245 alleles in the context of RWT4$^{Ca}$ (RWT4$^{Ca_Reg1}$: V123L/R124T, RWT4$^{Ca_Reg2}$: R627T) (Fig. 5b). A RWT4
246 variant incorporating the six-amino-acid extension at its C-terminus was also generated
247 (RWT4$^{Ca_+C\text{-}tail}$) (Fig. 5b). Subsequently, we evaluated the capacity of these RWT4 variants to
248 perceive AvrPWT4 for defense activation in rice protoplasts. Protoplasts transfected with wild-
249 type *Rwt4$^{Ca}$* and *AvrPwt4* displayed a significant reduction in cell viability (Fig. 5c). However, cells
250 transfected with the *Rwt4$^{Ca_Reg1}$* variant and *AvrPwt4* failed to show a decrease in viability (Fig.
251 5c). Similarly, no cell death was observed upon co-transfection of *Rwt4$^{Ca_+C\text{-}tail}$* with *AvrPwt4* (Fig.
252 5c). Cells expressing *Rwt4$^{Ca_Reg2}$* and *AvrPwt4* exhibited a comparable reduction in cell viability to
253 cells expressing *Rwt4$^{Ca}$* and *AvrPwt4* (Fig. 4C, $p<0.0001$). Western blotting confirmed the protein
254 expression of RWT4$^{Ca}$, RWT4$^{Ca_Reg1}$, RWT4$^{Ca_Reg2}$, and RWT4$^{Ca_C\text{-}tail}$ in rice protoplasts (Fig. S9a).
255 These findings highlight the importance of RWT4$^{Ca}$'s C-terminus and residues V124/R125 in the
256 KDup in defense activation (Fig. 5a, right).
257
258 To assess the impact of these residues on AvrPWT4 binding, yeast-two hybrid analyses was
259 conducted. As expected, RWT4$^{Ca}$ can interact with AvrPWT4 (Fig. 5d and S8b). However, a weak
260 interaction was observed between the susceptible variant from Chinese Spring, RWT4$^{Cs}$, and
261 AvrPWT4 (Fig. S9b). Next, we analyzed the interaction between RWT4 variant proteins and

262 AvrPWT4. No interaction was observed between RWT4$^{Ca_Reg1}$ and AvrPWT4, indicating that
263 V124/R125 in the integrated KDup is required for AvrPWT4 binding (Fig. 5d). The C-terminal
264 extension did not influence binding to AvrPWT4 (Fig. 5d). Western blot assays confirmed
265 expression of RWT4 and its variants in yeast (Fig. S9c). These data demonstrate that the binding
266 capacity of RWT4 to AvrPWT4 is required, but not sufficient for eliciting defense.
267

268 **Discussion**

269 TKPs have emerged as a novel class of non-canonical resistance proteins, representing ~10% of
270 the cloned *Triticeae* R genes [4,34]. Currently, TKPs conferring disease-resistance are exclusively
271 found in monocots [6]. In this study, we demonstrate the RWT4 TKP can be transferred and elicit
272 defense between wheat and rice. Furthermore, both RWT4 kinase activity and direct effector
273 binding are required for defense activation. It was hypothesized that TKP pseudokinase domains
274 acts as a decoy for effector binding, activating the kinase domain for downstream
275 phosphorylation or signaling [9]. Our results demonstrate that AvrPWT4 binds to both kinase and
276 pseudokinase regions. AvrPWT4 binding to both regions *in planta* may facilitate RWT4
277 intramolecular kinase interactions for activation (Fig. 5e). For plant receptor-like kinases, hetero-
278 dimerization is a common activation mechanism for signaling initiation [35].

279

280 TKP-mediated resistance is associated with the induction of cell death and robust defense
281 responses [6,14,22]. Like PRR and NLR immune receptors that can directly detect pathogen
282 components, RWT4 directly binds to AvrPWT4 and this binding is crucial for defense activation.
283 *Rwt4* is allelic to *Wtk3*, which confers resistance to powdery mildew disease caused by *Blumeria*
284 *graminis* f.sp. *tritici* [14,15]. Though highly similar in amino acid sequence, the effector targets of
285 WTK3 are currently unknown, and no ortholog of *Pwt4* is present in *B. graminis*. The majority of
286 functional TKPs conferring disease resistance belong to the LRR_8B kinase subfamily [9,10,16].
287 Prototypic members of this subfamily are cysteine-rich receptor-like kinases involved in plant
288 defense and can confer resistance to fungal pathogens [36,37].

289

290 Whether an NLR is involved in TKP signaling downstream of TKP-effector binding remains an open
291 question. Arabidopsis ZED1, a pseudokinase belonging to receptor-like cytoplasmic kinase (RLCK),
292 targets the *P. syringae* effector HopZ1[38]. This interaction is crucial for HopZ1 recognition by the
293 NLR ZAR1, leading to the formation of a resistance complex that activates immunity[38]. PBS1,
294 another Arabidopsis RLCK, acts as a decoy that activates the NLR PBS5 upon cleavage by the *P.*
295 *syringae* effector AvrPphB[39]. Although our results demonstrate that the direct binding of RWT4
296 to AvrPWT4 and RWT4 kinase activity are essential for eliciting immunity, the involvement of an

297 NLR in TKP-mediated defense cannot be ruled out. RWT4 retains effector recognition when
298 transferred between wheat and rice, indicating that an NLR may be ancient. The elucidation of
299 TKP immune complexes and direct downstream targets will reveal how these novel proteins
300 confer resistance.
301
302 *In vitro* kinase activity has been demonstrated for RPG1, WTK7-TM, and our work on the RWT4
303 TKP [10,19]. *In vitro*, the pseudokinase region does not inhibit the kinase activity of RPG1 and RWT4
304 [19]. We hypothesize that kinase activity is inhibited at a resting state *in planta* in the absence of
305 pathogen perception. RPG1 activation *in planta* is only observed in the presence of avirulent
306 spores of *P. graminis* [20], consistent with the hypothesis that TKPs rely on pathogen perception for
307 activation. Additional regions are also required for RWT4 full functionality such as the V123R124
308 sites for effector binding and the C-terminus (Fig. 4c and 4d).
309
310 The identified effector binding site V123R124 is within the integrated kinase duplication,
311 consistent with the hypothesis that KDup is an integrated domain (ID) for effector binding (Fig. 4
312 and 5b). IDs commonly found in NLRs include kinase, WRKY, Zinc-finger BED, and heavy metal-
313 associated (HMA) domains[18]. IDs facilitate NLRs to recognize sequence/structure-diverse
314 effectors that target to similar host proteins [40]. The HMA domain of rice Pik-1 directly binds to the
315 effector Avr-Pik1 for immune activation and the capability of effector binding contributes to
316 positive selection for Pik-1 alleles [41]. Similarly, in a companion paper Reveguk et al., (2024)
317 recently identified IDs are prevalent in TKPs found across the plant kingdom [8]. They also identified
318 an integrated HMA domain in the first TKP to be cloned, barley RPG1[8]. No other TKPs conferring
319 resistance aside from RWT4/WKT3 contain IDs that are partial kinase duplications. Thus, TKPs
320 conferring disease resistance may frequently employ diverse IDs to trap pathogen effectors.
321
322 Effector targeting of plant kinases is an important strategy to enhance pathogen virulence. The
323 *Pseudomonas syringae* AvrPtoB effector targets the plant kinase SnRK2.8, promoting pathogen
324 virulence upon SnRK2.8 phosphorylation [42]. The fungal NIS1 effector family from *Colletotrichum*
325 spp. and *Magnaporthe oryzae* act as kinase inhibitors, targeting the BAK1 and BIK1 kinases

326 required for effective defense mediated by multiple surface-localized receptors [43]. PWT4 has
327 canonical fungal effector features, including an N-terminal secretion signal and small size (75
328 amino acids) [23]. AvrPWT4 suppresses resistance conferred by RMG8, an MCTP kinase fused with
329 multiple C2 domains [25,44]. Thus, AvrPWT4 likely targets plant kinases to promote virulence in the
330 absence of RWT4. Accordingly, we hypothesize that KFPs serve both as receptors and decoys for
331 perception and deception of biotrophic fungal effectors that are aiming to suppress host kinases
332 involved in the activation of plant immunity [5].
333
334 TKPs have emerged as a novel class of resistance proteins that have been widely deployed to
335 control devastating biotrophic fungal pathogens [6,10,11,14,15]. Future investigations identifying
336 effector-TKP pairs as well as their phosphorylation targets will shed light into TKP activation and
337 signaling. This foundational information can facilitate receptor engineering and the deployment
338 of TKPs across diverse plant species.
339
340 **Online Methods**
341 ***Wheat infection assays***
342 Wheat seeds were pre-germinated on moistened filter papers. After 24 hours, sprouted seeds
343 were sown in the soil in seedling cases (5.5 × 15 × 10 cm, Sakata Prime Mix, Sakata Seed
344 Corporation, Yokohama, Japan), and grown at 22°C in a controlled-environment room with a 12-
345 h photoperiod of fluorescent lighting for eight days. Primary leaves of the nine-day-old seedlings
346 were fixed onto a hard plastic board with rubber bands just before inoculation. Conidial
347 suspensions ($1 \times 10^5$ conidia/mL) were prepared as described previously [45] and sprayed onto fixed
348 primary leaves using an air compressor. The inoculated seedlings were incubated in a tray sealed
349 with plastic wrap under dark and humid conditions at 22°C for 24 h, then transferred to dry
350 conditions with a 12-h photoperiod of fluorescent lighting and incubated at 22°C for an additional
351 3-5 days. Four to six days after inoculation, symptoms were evaluated based on the size and color
352 of lesions [46]. The size of lesions was rated on six progressive grades from 0-5: 0 = no visible
353 infection; 1 = pinhead spots; 2 = small lesions (<1.5 mm); 3 = scattered lesions of intermediate
354 size (<3 mm); 4 = large typical lesion; and 5 = complete blighting of leaf blades. A disease score

355 comprised a number denoting the lesion size and a letter indicating the lesion color: 'B' for brown
356 lesions and 'G' for green lesions. The infection types 0, 1B, and 2B were regarded as resistant,
357 while the infection types 3G, 4G, and 5G were considered susceptible (Table S1).
358
359 ***Cloning and site-directed mutagenesis***
360 The *Rwt4* Cadenza allele (*Rwt4*$^{Ca}$, TraesCAD_scaffold_040753_01G000200.1) and Chinese Spring
361 allele (*Rwt4*$^{Cs}$, TraesCS1D02G058900) were codon-optimized for expression in rice and
362 synthesized (Twist Bioscience gene fragment). *Rwt4*$^{Ca_K217R/K327R}$ was generated by PCR-based site-
363 directed mutagenesis. Genes of interest were cloned to Gateway™ pENTR™ 4 Dual Selection
364 Vector (A10465) by NEBuilder HiFi DNA Assembly Master Mix (NEB, E2621L) and cloned to a
365 pUC19 expression vector powered by the maize ubiquitin promoter (*Zm*UBI) via Gateway LR
366 reaction. Full length of *Rwt4*$^{Ca}$, its kinase region, and pseudokinase region were cloned into *E. coli*
367 expression plasmids pET28a-His-MBP [47] or pET28a-His (EMD Biosciences) using ligation-
368 independent cloning (LIC) for recombinant protein production [48].
369
370 We refer to the *Pwt4* effector in two terms, the avirulent allele that can be recognized by *Rwt4*
371 (*AvrPwt4*) and a virulent form that cannot be recognized (*VirPwt4*) [23]. *AvrPwt4* (*Pwt4-Br58* type
372 allele, GeneBank:LC202655.1) and *VirPwt4* (*Pwt4-Br48* type allele, GenBank: LC202656.1), lacking
373 their N-terminal signal peptide as predicted by SignalP 5.0
374 (https://services.healthtech.dtu.dk/services/SignalP-5.0/), were codon optimized, synthesized
375 (Twist Bioscience gene fragment) and cloned into the pUC19:*Zm*UBI expression vector via
376 Gateway LR reaction. *AvrPwt4* and *VirPwt4* were cloned into an *E. coli* expression plasmid pET28a-
377 GST using ligation-independent cloning (LIC) for recombinant protein purification [48,49]. Sequences
378 were validated by whole plasmid sequencing service (Plasmidsaurus). All constructs and primers
379 used in this study are listed in Table S5 and Table S6.
380
381 **RWT4 domain architecture prediction**
382 RWT4$^{Ca}$ protein architecture was predicted via InterPro (https://www.ebi.ac.uk/interpro)[32]. KDup
383 was identified based on InterPro annotation and further defined by aligning the partial kinase

384 sequence (amino acids 1-142; nucleotides 117-426) and the kinase domain (amino acids 189-240;
385 nucleotides 567-720). The linker region was defined based on Alphafold structure modeling[50].
386 The cDNA and amino acid sequences of RWT4$^{Ca}$ were aligned with Clustal Omega Multiple
387 Sequence Alignment (MSA) server (https://www.ebi.ac.uk/jdispatcher/msa/clustalo) and dot
388 plots were generated with the program Dotter obtained from Ubuntu repositories
389 (https://packages.ubuntu.com/)[51].
390
391 ***Recombinant protein expression and purification***
392 Full length RWT4$^{Ca}$, the kinase region (K, 1-478 amino acids), and the pseudokinase region (PK,
393 540-914 amino acids) were expressed in *E. coli* BL21 Rosetta (DE3) strain and purified by affinity
394 and size exclusion chromatography. Four liters of cells were grown at 37$^{o}$C to $OD_{600}$ of 0.4 before
395 adding IPTG to a final concentration of 0.5 mM. Cells were resuspended in a lysis buffer consisting
396 of 50 mM HEPES pH 8.5, 300 mM NaCl, 1 mM PMSF (phenylmethylsulfonyl fluoride) and 1 µg/mL
397 DNase and lysed by a microfluidizer at 18k psi. The lysate was then clarified by centrifugation at
398 16000 g at 4$^{o}$C for 50 min. The proteins of interest were separated from the clarified lysate by
399 immobilized metal affinity chromatography (IMAC) and eluted with an elution buffer (50 mM
400 HEPES at pH 8.5, 300 mM NaCl and 250 mM imidazole) on an AKTA FPLC. Eluted samples were
401 dialyzed into a low-salt buffer (20 mM Tris-HCl, pH 8.5, 200 mM NaCl) for further affinity-based
402 purification using 1 mL MBPTrapHP columns (Cytiva Life Science, #29048641). Target proteins
403 were eluted by a buffer (10 mM maltose, 20 mM Tris-HCl, pH 8.5, 200 mM NaCl) and were injected
404 to a HiLoad 16/600 Superdex 200 PG column equilibrated with 10 mM HEPES at pH 8.0 and 150
405 mM NaCl. Fractions corresponding to the proteins of interest were collected and visualized by
406 Coomassie-stained SDS-PAGE, before being concentrated using a 3 kDa MWCO Amicon Ultra
407 centrifugal filter (Millipore Sigma, #UFC9003) to appropriate concentrations for further analysis.
408
409 AvrPWT4 and VirPWT4 were expressed in *E. coli* BL21 Rosetta (DE3) and purified by affinity and
410 size exclusion chromatography. Their expression and cell lysates were prepared as described
411 above. Cell lysates were purified by affinity-based chromatography using 1mL GSTrap HP columns
412 (Cytiva Life Science, #17528201) equilibrated with a binding buffer 140 mM NaCl, 2.7 mM KCl, 10

413 mM $Na_2HPO_4$, 1.8 mM $KH_2PO_4$, pH 8.0. Target proteins were eluted with elution buffer (50 mM
414 Tris-HCl, 10 mM reduced glutathione, pH 8.0) and dialyzed to a buffer condition (10 mM Tris-HCl
415 pH 8.0, 150 mM NaCl, 0.5 mM EDTA, 1 mM DTT) optimized for TEV protease cleavage (ProTEV
416 Plus, Promega, V6101). Samples were adjusted to a final volume of 10 mL with 100U TEV protease
417 and incubated at 4$^{o}$C for overnight. After the incubation, samples were loaded into a GSTrap HP
418 column (Cytiva Life Science, #17528201), and the flow-through was collected for further size
419 exclusion chromatography (HiLoad 16/600 Superdex 200 PG column) as described above. Purified
420 proteins were visualized by Coomassie-stained SDS-PAGE and concentrated using a 3 kDa MWCO
421 Amicon Ultra centrifugal filter (Millipore Sigma, #UFC9003).
422
423 ***Kinase activity and phosphatase assays***
424 Kinase reactions were performed according to Lin and their colleagues with minor modifications
425 [52]. Kinase reactions were performed in a kinase buffer consisting of 20 mM Tris-HCl (pH 7.5), 10
426 mM $MgCl_2$, 1 mM $CaCl_2$, 1 mM dithiothreitol, 100 µM ATP, with additional 10 µCi of [$^{32}$P]γATP
427 (Revvity, #BLU002A100UC). Two µg of recombinant protein was mixed with the mentioned buffer
428 and reactions were incubated at 30$^{o}$C for 30 min and stopped with 3x Laemmli sample buffer.
429 Radioactive samples were separated on SDS-PAGE gels and visualized by autoradiography. For
430 trans-phosphorylation assays, RWT4$^{Ca}$ and PWT4 were mixed at 1:1 ratio and incubated on ice for
431 20 min before the mentioned kinase reaction. For phosphatase treatments, 2 µg of recombinant
432 protein was mixed with 400U lambda protein phosphatase (NEB, #P0753S) at 30$^{o}$C for 30 min
433 before separated by an SDS-PAGE. The phosphorylation status of RWT4 was visualized by a
434 Western blot using an Phospho-Threonine/Tyrosine Antibody (Cell signaling technology, #9381)
435 at 1:2000 dilution in a TBST buffer for an overnight incubation at 4$^{o}$C. The antibody was detected
436 by an Immun-Star Goat Anti-Rabbit (GAR)-HRP Conjugate (Bio-Rad #1705046) and protein signals
437 were detected on the immunoblot using SuperSignal™ West Pico PLUS Chemiluminescent
438 Substrate (ThermoFisher Scientific #34580) and visualized by ChemiDoc™ Touch Gel Imaging
439 System (Bio-Rad #1708370).
440
441 ***Mass spectrometry (MS)***

442 Kinase reactions using 6 µg of RWT4$^{Ca}$ and AvrPWT4 were conducted as described above. Samples
443 were treated with freshly prepared 10 mM dithiothreitol and 55 mM Iodoacetamide for reduction
444 and alkylation. Samples were digested by using trypsin at 10 ng/µL at 37$^{o}$C overnight and peptides
445 were harvested by with 50% ACN/0.1% FA (formic acid, Sigma #06473), lyophilized and
446 resuspended with 0.1% FA. Samples were submitted to the Genomics Center Proteomics Core at
447 the University of California, Davis. Reverse-phased Liquid Chromatography (LC) was performed
448 on an EASY-nLC II HPLC (Thermofisher Scientific). The digested peptides were desalted by ZipTip
449 with 0.6 µL C18 resin (ZTC18S096, Millipore) before separated by a 75-µm × 150-mm C18 100A 3-
450 units reverse phased column at a flow rate 300 nL/min. The gradient elution employed buffer A
451 (0.1% formic acid) and buffer B (100% acetonitrile) over 60 min, transitioning from 5% to 35%
452 buffer B over 45 min, followed by a 35% to 80% buffer B gradient over 5 min, holding at 80%
453 buffer B for 2 min, and finally returning to 5% buffer B over 2 min, maintaining at 5% buffer B for
454 6 min before the next sample injection.
455
456 Mass spectra were collected on an Orbitrap Exploris Mass Spectrometer (ThermoFisher Scientifics)
457 with one full scan (300–1,600 m/z, R = 60,000 at 200 m/z) at a target of 3x $10^6$ ions, followed by
458 data-independent MS/MS scans with higher-energy collisional dissociation (HCD) detected in the
459 Orbitrap (R = 15,000 at 200 m/z). Results were analyzed by using the DIA-NN software package [53].
460 The phosphorylated peptides were mapped to the sequence of RWT4$^{Ca}$ and AvrPWT4. Peptide
461 spectra were visualized by using Skyline software package [54].
462
463 ***Bio-Layer Interferometry (BLI)***
464 BLI experiments were conducted by using the ForteBio Octet® RED384 equipment at the UC Davis
465 Octet® Real-Time Drug and Protein Binding Kinetics Unit. Analyte proteins (His-RWT4$^{Ca}$, MBP-His-
466 RWT4$^{Ca}$, MBP-His-K and MBP-His-PK) were diluted to 100nM in Octet® Kinetics Buffer (SARTORIUS,
467 #18-1105) for immobilized to Octet® Ni-NTA (NTA) Biosensors (SARTORIUS, #18-5101). Ligand
468 proteins (AvrPWT4 and VirPWT4, without tags, or GST) were prepared at 10 µM in Octet® Kinetics
469 Buffer as a stock solution for a 1.5x serial dilution to generate concentration gradient. Wavelength

470 measurement for the interaction between ligand and analyte proteins followed the
471 manufacturer's protocol with 600 sec for association and 600 sec for dissociation [55].
472
473 ***Yeast-two hybrid (Y2H)***
474 To validate RWT4 and PWT4 interactions, *Rwt4*$^{Ca}$ and its variant proteins were cloned into the
475 prey vector pGADT7 (Takara, #630442) while *AvrPwt4* and *VirPwt4* were cloned into the bait
476 vector pGBKT7 (Takara, #630443). These constructs were co-transformed into the yeast strain
477 AH109 following the manufacturer's instructions from Frozen-EZ Yeast Transformation II™ (Zymo
478 Research). Yeast transformation was tested by dilution plating cells from a starting concentration
479 of $OD_{600}$ 5.0 on double drop out (DDO) plates (SD-2: SD/-Trp/-Leu), while interactions were
480 confirmed through quadruple drop out (QDO) selection (SD-4: SD/-Trp/-Leu/-His/-Ade/3-AT). 3-
481 AT (3-amino-1,2,4-triazole) was used at 10 mM to reduce background HIS activation. The
482 transformed yeast cells were incubated at 30$^{o}$C for two to five days before imaging.
483
484 For protein expression in yeast cells, five mL of yeast cells containing the genes of interest were
485 grown at 30$^{o}$C for overnight in SD-2 and harvested by centrifuging at 5000 rpm for 10 min. Cell
486 pellets were resuspended in a lysis buffer (150 mM NaCl, 10 mM HEPES, pH 7.5) with Pierce™
487 Protease Inhibitor (ThermoFisher Scientific #A32965) as suggested by the manual. Resuspended
488 cells were mixed with acid-washed glass beads (Sigma #G8772) and lysed by sonication for 5 min.
489 Soluble proteins were separated by centrifuging at 13000 rpm for 10 min, mixed with 3x laemmli
490 buffer, and resolved by SDS-PAGE gels and transferred to PVDF membranes (Bio-Rad #1620177)
491 for western blotting. Monoclonal ANTI-FLAG® M2-Peroxidase (HRP) antibody was used at 1:2000
492 (Millipore Sigma, A8592) dilution in a TBST buffer and incubated at 4$^{o}$C overnight. Protein signals
493 were detected by using SuperSignal™ West Pico PLUS Chemiluminescent Substrate
494 (ThermoFisher Scientific #34580) and visualized by ChemiDoc™ Touch Gel Imaging System (Bio-
495 Rad).
496
497 ***Co-immunoprecipitation assays***

498 To confirm the *in-planta* interaction of RWT4$^{Ca}$ and AvrPWT4, we performed *Agrobacterium*
499 *tumefaciens*-mediated transient expression in *Nicotiana benthamiana*. *Rwt4$^{Ca}$* was cloned to a
500 dexamethasone-inducible system (pTA7001, [56]) with a C-terminal 3xFLAG tag, while *AvrPwt4* and
501 *VirPwt4* were cloned to pTA7001 vector with a GFP tag. The cloned constructs were transformed
502 into the *A. tumefaciens* C58C1 strain and infiltrated into four-week *N. benthamiana* at an $OD_{600}$ =
503 0.3 for each construct. Twenty-four hours post-infiltration, 30 µM dexamethasone solution
504 containing 0.01% Triton X-100 was applied to the leaf surface and two grams of leaf tissue was
505 harvested 16 hours after dexamethasone application.
506
507 For immunoprecipitation, leaf tissue was ground in liquid nitrogen and resuspended in 2 mL IP
508 buffer (50mM Tris-HCl ph7.5, 150mM NaCl, 0.1% Triton, 0.2% NP-40) containing 1× complete
509 protease inhibitor (Thermo Fisher Scientific #A32963). Samples were centrifuged at 14000 rpm
510 for 10 min to remove tissue debris. The supernatant was incubated with 20 µL of ChromoTek GFP-
511 Trap® Agarose (Proteintech, # AB_2631357) at 4°C for 1 hour. Samples were washed five times
512 with high stringency wash buffer (50mM Tris-HCl ph7.5, 300mM NaCl, 0.1% Triton, 0.2% NP-40),
513 resuspended in 3x laemmli buffer, resolved by SDS-PAGE and transferred to PVDF membranes
514 (Bio-Rad # 1620177) for immunoblotting. Monoclonal ANTI-FLAG® M2-Peroxidase (HRP) antibody
515 (Millipore Sigma, A8592) or GFP Antibody, HRP (Miltenyi Biotec, # 130-091-833) were diluted at
516 1:2000 in a TBST buffer and incubated at 4°C for overnight. Protein signals were detected by using
517 SuperSignal™ West Pico PLUS Chemiluminescent Substrate (ThermoFisher Scientific #34580) and
518 visualized by ChemiDoc™ Touch Gel Imaging System (Bio-Rad).
519
520 ***Rice protoplast transformation and cell viability assay***
521 Protoplasts were prepared according to [57], with modifications. Seeds of the rice cultivar Kitaake
522 (*Oryza sativa*) were surface sterilized and grown on ½ MS media at 25°C in dark for 12 days before
523 transitioning to a photoperiod of 12 h light (approximately 150 µmol $m^{-2}$ $s^{-1}$) and of 12 h darkness
524 for two days. Rice plants were cut into approximately 1 mm strips and immediately transferred
525 into 0.6 M mannitol for 10 min in the dark.
526

527 The rice strips were then incubated with an enzyme solution (1.5% Cellulase RS, 0.75%
528 Macerozyme R-10, 0.6 M mannitol, 10 mM MES at pH 5.7, 10 mM $CaCl_2$ and 0.1% BSA) for 5 h in
529 the dark with gentle shaking at 40 rpm. The enzymatic digestion was stopped by adding an equal
530 volume of W5 solution (154 mM NaCl, 125 mM $CaCl_2$, 5 mM KCl and 2 mM MES at pH 5.7),
531 followed by a gentle shaking by hands for 10 seconds. Protoplasts were released and washed
532 through 40 µm nylon mesh into round-bottom tubes three times using W5 solution. The washed
533 protoplasts were harvested by centrifugation at 380 g for 10 min, and pellets were resuspended
534 in MMG solution (0.4 M mannitol, 15 mM $MgCl_2$, and 4 mM MES at pH 5.7) at a concentration of
535 $6 \times 10^6$ cells/mL, determined using a hematocytometer.
536
537 For protoplast transfection, 10 µg of plasmid DNA was mixed with 100 µL of the protoplasts and
538 100 µL freshly prepared PEG solution [40% (W/V) PEG 4000; Sigma, 0.2 M mannitol, and 0.1 M
539 $CaCl_2$]. The mixed samples were incubated in the dark for 20 min at room temperature. After
540 incubation, 2 mL W5 solution was added to stop the transfection, and protoplasts were pelleted
541 by centrifugation at 380 g for 10 min. The protoplasts were resuspended in 1 mL fresh W5 solution
542 and cultured in the dark for 16 h for cell viability assay or 4 h for detecting protein expression.
543
544 Protein expression from protoplasts were assayed by pull-down assay and Western blot. Four
545 individual transfection events (equals to $2.4 \times 10^6$ cells) were collected and harvested by
546 centrifugation at 380 g for 5 min. Cell pellets were resuspended with a lysis buffer (150 mM NaCl,
547 10 mM HEPES, pH 7.5) containing Pierce™ Protease Inhibitor (ThermoFisher Scientific #A32965)
548 as suggested by the manual. Cells were lysed by strong vortex for 5 min and mixed with 20 µL of
549 Pierce™ Anti-DYKDDDDK Magnetic Agarose (Thermo Scientific™, #A36797). The mixtures were
550 incubated at 4°C for two hours and wash for three times with the lysis buffer as suggested by the
551 manual. Samples were mixed with 3x laemmli buffer and resolved by SDS-PAGE gels and
552 transferred to PVDF membranes (Bio-Rad # 1620177) for immune blotting. Monoclonal ANTI-
553 FLAG® M2-Peroxidase (HRP) antibody (Millipore Sigma, A8592) was used at 1:2000 dilution in a
554 TBST buffer and incubated at 4°C for overnight. Protein signals were detected by using

555 SuperSignal™ West Pico PLUS Chemiluminescent Substrate (ThermoFisher Scientific #34580) and
556 visualized by ChemiDoc™ Touch Gel Imaging System (Bio-Rad).
557
558 ***Cell viability assay***
559 Protoplast cell viability was assayed using the CellTiter-Glo® 2.0 Cell Viability Assay kit (Promega,
560 #G9241) as instructed by the manual and by [58]. In brief, 100 µL of protoplasts resuspended in W5
561 were mixed with 100 µL of the CellTiter-Glo reagent in a 96-well white assay plate. The samples
562 were mixed at orbital shaker for five minutes and then incubated in the dark for 10 min at room
563 temperature prior to recording the luminescent signal. Luminescence was measured using the
564 TriStar LB 941 Multimode Microplate Reader and MikroWin 2000 software (Berthold).
565
566 ***RNA extraction and qPCR***
567 Total RNA was extracted from rice protoplasts seven hours after transfection by using the
568 PicoPure™ RNA Isolation Kit (ThermoFisher Scientific, #KIT0204) with on-column DNase
569 treatment as per manual instructed. First-strand cDNA was synthesized using M-MLV Reverse
570 Transcriptase (Promega, #M1701) with an oligo d(T) primer at 25 µg/mL. The transcripts of
571 defense marker genes were quantified by using iTaq™ Universal SYBR® Green One-Step Kit (BIO-
572 RAD, #1725150) with 40 cycles of 1 s at 95°C and 30 s at 60°C.
573
574 **Data analyses and availability**
575 For protoplast viability assays, at least five independent transfection events were used as
576 biological replicates, and the presented results are representative of at least three independent
577 experiments. For qPCR of defense gene activation, four independent transfection events were
578 used. Statistical differences were detected using one way ANOVA coupled with a Tukey HSD post-
579 hoc test, $\alpha = 0.05$. Protein assays including kinase activity tests, western blot, co-
580 immunoprecipitation, and yeast-two hybrid were independently repeated at least twice with
581 similar results. All materials are available from the corresponding author upon request. Raw data
582 underlying each figure are available at https://doi.org/10.5281/zenodo.11087676.
583

584 **References:**


585 1 Dodds, P. N. & Rathjen, J. P. Plant immunity: towards an integrated view of plant-pathogen
586 interactions. *Nat Rev Genet* **11**, 539-548 (2010). https://doi.org:10.1038/nrg2812
587 2 Chiang, Y.-H. & Coaker, G. Effector Triggered Immunity: NLR Immune Perception and
588 Downstream Defense Responses. *The Arabidopsis Book* **2015** (2015).
589 3 Couto, D. & Zipfel, C. Regulation of pattern recognition receptor signalling in plants. *Nat*
590 *Rev Immunol* **16**, 537-552 (2016). https://doi.org:10.1038/nri.2016.77
591 4 Sanchez-Martin, J. & Keller, B. NLR immune receptors and diverse types of non-NLR
592 proteins control race-specific resistance in Triticeae. *Curr Opin Plant Biol* **62**, 102053
593 (2021). https://doi.org:10.1016/j.pbi.2021.102053
594 5 Fahima, T. & Coaker, G. Pathogen perception and deception in plant immunity by kinase
595 fusion proteins. *Nat Genet* **55**, 908-909 (2023). https://doi.org:10.1038/s41588-023-
596 01396-w
597 6 Klymiuk, V. *et al.* Cloning of the wheat Yr15 resistance gene sheds light on the plant
598 tandem kinase-pseudokinase family. *Nat Commun* **9**, 3735 (2018).
599 https://doi.org:10.1038/s41467-018-06138-9
600 7 Yu, G. *et al.* Aegilops sharonensis genome-assisted identification of stem rust resistance
601 gene Sr62. *Nat Commun* **13**, 1607 (2022). https://doi.org:10.1038/s41467-022-29132-8
602 8 Reveguk T., F. A., Potapenko E. , Reveguk I, Sela H., Klymiuk V., Li Y., Pozniak C., Wicker T.,
603 Coaker G.L., Fahima T. Atlas of tandem kinase proteins across the plant kingdom
604 *Submitted to Nat genet* (2024).
605 9 Klymiuk, V., Coaker, G., Fahima, T. & Pozniak, C. J. Tandem Protein Kinases Emerge as New
606 Regulators of Plant Immunity. *Mol Plant Microbe Interact* **34**, 1094-1102 (2021).
607 https://doi.org:10.1094/MPMI-03-21-0073-CR
608 10 Li, M. *et al.* A membrane associated tandem kinase from wild emmer wheat confers
609 broad-spectrum resistance to powdery mildew. *Nat Commun* **15**, 3124 (2024).
610 https://doi.org:10.1038/s41467-024-47497-w
611 11 Brueggeman, R. *et al.* The barley stem rust-resistance gene Rpg1 is a novel disease-
612 resistance gene with homology to receptor kinases. *Proc Natl Acad Sci U S A* **99**, 9328-
613 9333 (2002). https://doi.org:10.1073/pnas.142284999
614 12 Chen, S. *et al.* Wheat gene Sr60 encodes a protein with two putative kinase domains that
615 confers resistance to stem rust. *New Phytol* **225**, 948-959 (2020).
616 https://doi.org:10.1111/nph.16169
617 13 Gaurav, K. *et al.* Population genomic analysis of Aegilops tauschii identifies targets for
618 bread wheat improvement. *Nat Biotechnol* (2021). https://doi.org:10.1038/s41587-021-
619 01058-4
620 14 Lu, P. *et al.* A rare gain of function mutation in a wheat tandem kinase confers resistance
621 to powdery mildew. *Nat Commun* **11**, 680 (2020). https://doi.org:10.1038/s41467-020-
622 14294-0
623 15 Arora, S. *et al.* A wheat kinase and immune receptor form host-specificity barriers against
624 the blast fungus. *Nat Plants* **9**, 385-392 (2023). https://doi.org:10.1038/s41477-023-
625 01357-5

16 Wang, Y. *et al.* An unusual tandem kinase fusion protein confers leaf rust resistance in wheat. *Nat Genet* **55**, 914-920 (2023). https://doi.org:10.1038/s41588-023-01401-2

17 Yu, G. *et al.* The wheat stem rust resistance gene Sr43 encodes an unusual protein kinase. *Nat Genet* **55**, 921-926 (2023). https://doi.org:10.1038/s41588-023-01402-1

18 Marchal, C., Michalopoulou, V. A., Zou, Z., Cevik, V. & Sarris, P. F. Show me your ID: NLR immune receptors with integrated domains in plants. *Essays Biochem* **66**, 527-539 (2022). https://doi.org:10.1042/Ebc20210084

19 Nirmala, J. *et al.* Subcellular localization and functions of the barley stem rust resistance receptor-like serine/threonine-specific protein kinase Rpg1. *Proc Natl Acad Sci U S A* **103**, 7518-7523 (2006). https://doi.org:10.1073/pnas.0602379103

20 Nirmala, J., Drader, T., Chen, X., Steffenson, B. & Kleinhofs, A. Stem rust spores elicit rapid RPG1 phosphorylation. *Mol Plant Microbe Interact* **23**, 1635-1642 (2010). https://doi.org:10.1094/MPMI-06-10-0136

21 Lolle, S., Stevens, D. & Coaker, G. Plant NLR-triggered immunity: from receptor activation to downstream signaling. *Curr Opin Immunol* **62**, 99-105 (2020). https://doi.org:10.1016/j.coi.2019.12.007

22 Nirmala, J. *et al.* Concerted action of two avirulent spore effectors activates Reaction to Puccinia graminis 1 (Rpg1)-mediated cereal stem rust resistance. *Proc Natl Acad Sci U S A* **108**, 14676-14681 (2011). https://doi.org:10.1073/pnas.1111771108

23 Inoue, Y. *et al.* Evolution of the wheat blast fungus through functional losses in a host specificity determinant. *Science* **357**, 80-83 (2017). https://doi.org:10.1126/science.aam9654

24 Hossain, M. M. Wheat blast: A review from a genetic and genomic perspective. *Front Microbiol* **13**, 983243 (2022). https://doi.org:10.3389/fmicb.2022.983243

25 O'Hara, T. *et al.* The wheat powdery mildew resistance gene Pm4 also confers resistance to wheat blast. *bioRxiv*, 2023.2009.2026.559489 (2023). https://doi.org:10.1101/2023.09.26.559489

26 Asuke, S. *et al.* Evolution of wheat blast resistance gene Rmg8 accompanied by differentiation of variants recognizing the powdery mildew fungus. *bioRxiv*, 2023.2009.2026.559445 (2023). https://doi.org:10.1101/2023.09.26.559445

27 De Kesel, J., Gomez-Rodriguez, R., Bonneure, E., Mangelinckx, S. & Kyndt, T. The Use of PTI-Marker Genes to Identify Novel Compounds that Establish Induced Resistance in Rice. *Int J Mol Sci* **21** (2020). https://doi.org:10.3390/ijms21010317

28 Huang, L. F. *et al.* Multiple Patterns of Regulation and Overexpression of a Ribonuclease-Like Pathogenesis-Related Protein Gene, OsPR10a, Conferring Disease Resistance in Rice and Arabidopsis. *PLoS One* **11**, e0156414 (2016). https://doi.org:10.1371/journal.pone.0156414

29 Takeuchi, K. *et al.* RSOsPR10 expression in response to environmental stresses is regulated antagonistically by jasmonate/ethylene and salicylic acid signaling pathways in rice roots. *Plant Cell Physiol* **52**, 1686-1696 (2011). https://doi.org:10.1093/pcp/pcr105

30 Zulawski, M., Schulze, G., Braginets, R., Hartmann, S. & Schulze, W. X. The Arabidopsis Kinome: phylogeny and evolutionary insights into functional diversification. *Bmc Genomics* **15** (2014). https://doi.org:https://doi.org/10.1186/1471-2164-15-548

31 Piya, S. *et al.* Kinase-dead mutation: A novel strategy for improving soybean resistance to soybean cyst nematode Heterodera glycines. *Mol Plant Pathol* **23**, 417-430 (2022). https://doi.org:10.1111/mpp.13168

32 Paysan-Lafosse, T. *et al.* InterPro in 2022. *Nucleic Acids Res* **51**, D418-D427 (2023). https://doi.org:10.1093/nar/gkac993

33 Evans, R. *et al.* Protein complex prediction with AlphaFold-Multimer. *bioRxiv*, 2021.2010.2004.463034 (2022). https://doi.org:10.1101/2021.10.04.463034

34 Chen, R., Gajendiran, K. & Wulff, B. B. H. R we there yet? Advances in cloning resistance genes for engineering immunity in crop plants. *Current Opinion in Plant Biology* **77**, 102489 (2024). https://doi.org:https://doi.org/10.1016/j.pbi.2023.102489

35 Bender, K. W. & Zipfel, C. Paradigms of receptor kinase signaling in plants. *Biochem J* **480**, 835-854 (2023). https://doi.org:10.1042/BCJ20220372

36 Saintenac, C. *et al.* A wheat cysteine-rich receptor-like kinase confers broad-spectrum resistance against Septoria tritici blotch. *Nat Commun* **12**, 433 (2021). https://doi.org:10.1038/s41467-020-20685-0

37 Yadeta, K. A. *et al.* A Cysteine-Rich Protein Kinase Associates with a Membrane Immune Complex and the Cysteine Residues Are Required for Cell Death. *Plant Physiol* **173**, 771-787 (2017). https://doi.org:10.1104/pp.16.01404

38 Lewis, J. D. *et al.* The Arabidopsis ZED1 pseudokinase is required for ZAR1-mediated immunity induced by the Pseudomonas syringae type III effector HopZ1a. *Proc Natl Acad Sci U S A* **110**, 18722-18727 (2013). https://doi.org:10.1073/pnas.1315520110

39 Zhang, J. *et al.* Receptor-like cytoplasmic kinases integrate signaling from multiple plant immune receptors and are targeted by a Pseudomonas syringae effector. *Cell Host Microbe* **7**, 290-301 (2010). https://doi.org:10.1016/j.chom.2010.03.007

40 Maidment, J. H. R. *et al.* Effector target-guided engineering of an integrated domain expands the disease resistance profile of a rice NLR immune receptor. *Elife* **12** (2023). https://doi.org:ARTN e8112310.7554/eLife.81123

41 Bialas, A. *et al.* Two NLR immune receptors acquired high-affinity binding to a fungal effector through convergent evolution of their integrated domain. *Elife* **10** (2021). https://doi.org:ARTN e6696110.7554/eLife.66961

42 Lei, L., Stevens, D. M. & Coaker, G. Phosphorylation of the Pseudomonas Effector AvrPtoB by Arabidopsis SnRK2.8 Is Required for Bacterial Virulence. *Mol Plant* **13**, 1513-1522 (2020). https://doi.org:10.1016/j.molp.2020.08.018

43 Irieda, H. *et al.* Conserved fungal effector suppresses PAMP-triggered immunity by targeting plant immune kinases. *Proc Natl Acad Sci U S A* **116**, 496-505 (2019). https://doi.org:10.1073/pnas.1807297116

44 Inoue, Y., Vy, T. T. P., Tani, D. & Tosa, Y. Suppression of wheat blast resistance by an effector of Pyricularia oryzae is counteracted by a host specificity resistance gene in wheat. *New Phytol* **229**, 488-500 (2021). https://doi.org:10.1111/nph.16894

45 Tagle, A. G., Chuma, I. & Tosa, Y. Rmg7, a New Gene for Resistance to Triticum Isolates of Pyricularia oryzae Identified in Tetraploid Wheat. *Phytopathology* **105**, 495-499 (2015). https://doi.org:10.1094/PHYTO-06-14-0182-R

46 Hyon, G. S. *et al.* Characterization of interactions between barley and various host-specific subgroups of *Magnaporthe oryzae* and *M-grisea*. *J Gen Plant Pathol* **78**, 237-246 (2012). https://doi.org:10.1007/s10327-012-0386-6

47 Currinn, H., Guscott, B., Balklava, Z., Rothnie, A. & Wassmer, T. APP controls the formation of PI(3,5)P(2) vesicles through its binding of the PIKfyve complex. *Cell Mol Life Sci* **73**, 393-408 (2016). https://doi.org:10.1007/s00018-015-1993-0

48 Eschenfeldt, W. H., Lucy, S., Millard, C. S., Joachimiak, A. & Mark, I. D. A family of LIC vectors for high-throughput cloning and purification of proteins. *Methods Mol Biol* **498**, 105-115 (2009). https://doi.org:10.1007/978-1-59745-196-3_7

49 Shabek, N. *et al.* Structural insights into DDA1 function as a core component of the CRL4-DDB1 ubiquitin ligase. *Cell Discov* **4** (2018). https://doi.org:https://doi.org/10.1038/s41421-018-0064-8

50 Jumper, J. *et al.* Highly accurate protein structure prediction with AlphaFold. *Nature* **596**, 583-589 (2021). https://doi.org:10.1038/s41586-021-03819-2

51 Madeira, F. *et al.* Search and sequence analysis tools services from EMBL-EBI in 2022. *Nucleic Acids Res* **50**, W276-W279 (2022). https://doi.org:10.1093/nar/gkac240

52 Lin, Z. J., Liebrand, T. W., Yadeta, K. A. & Coaker, G. PBL13 Is a Serine/Threonine Protein Kinase That Negatively Regulates Arabidopsis Immune Responses. *Plant Physiol* **169**, 2950-2962 (2015). https://doi.org:10.1104/pp.15.01391

53 Demichev, V., Messner, C. B., Vernardis, S. I., Lilley, K. S. & Ralser, M. DIA-NN: neural networks and interference correction enable deep proteome coverage in high throughput. *Nat Methods* **17**, 41-44 (2020). https://doi.org:10.1038/s41592-019-0638-x

54 MacLean, B. *et al.* Skyline: an open source document editor for creating and analyzing targeted proteomics experiments. *Bioinformatics* **26**, 966-968 (2010). https://doi.org:10.1093/bioinformatics/btq054

55 Shah, N. B. & Duncan, T. M. Bio-layer interferometry for measuring kinetics of protein-protein interactions and allosteric ligand effects. *J Vis Exp*, e51383 (2014). https://doi.org:10.3791/51383

56 Gu, Y. & Innes, R. W. The KEEP ON GOING protein of Arabidopsis recruits the ENHANCED DISEASE RESISTANCE1 protein to trans-Golgi network/early endosome vesicles. *Plant Physiol* **155**, 1827-1838 (2011). https://doi.org:10.1104/pp.110.171785

57 He, F., Chen, S., Ning, Y. & Wang, G. L. Rice (Oryza sativa) Protoplast Isolation and Its Application for Transient Expression Analysis. *Curr Protoc Plant Biol* **1**, 373-383 (2016). https://doi.org:10.1002/cppb.20026

58 Wang, J. *et al.* Reconstitution and structure of a plant NLR resistosome conferring immunity. *Science* **364** (2019). https://doi.org:10.1126/science.aav5870

**Acknowledgements:**

This research is supported by grants from the United States National Science Foundation (1937855) and the United States Department of Agriculture (2020-67013-32577) to GC and the United States-Israel Binational Science Foundation (BSF, 2019654) to TF and the Swiss National Science Foundation (310030_204165) to BK. MS analysis was carried out at the Genomics Center Proteomics Core at the University of California, Davis. The kinase assay using [$^{32}$P]γATP was conducted in the facility established by Dr. Yen-Wen Kuo, Department of Plant Pathology at the University of California, Davis. BLI experiments were performed in the Cortopassi Lab with technical assistance from Dr. Alexey Tomilov at the University of California, Davis. Rice Kitaake seeds were provided by Dr. Pamela Ronald, Department of Plant Pathology at the University of California, Davis. The pUC19::Zm*UBI* plasmid was provided by Dr. Jorge Dubcovsky from the Department of Plant Science, University of California, Davis. The pET28s::GST vector was provided by Dr. Nitzan Shabek, Department of Plant Biology, University of California, Davis.

**Author contributions**

Y-CS and GC designed the study with assistance from TZ and BK. SA performed wheat inoculation experiments, YL performed yeast-two hybrid, ZB identified KDup, SB assisted with molecular cloning, *Agrobacterium*-mediated expression in *N. benthamiana* and western blotting under the guidance of Y-CS and GC. Y-CS performed all other experiments and data analyses. Y-CS and GC wrote the original draft and all authors reviewed and edited the manuscript.

**Ethics declarations**

The authors declare no competing interests.

773 **Figures and figure legends**

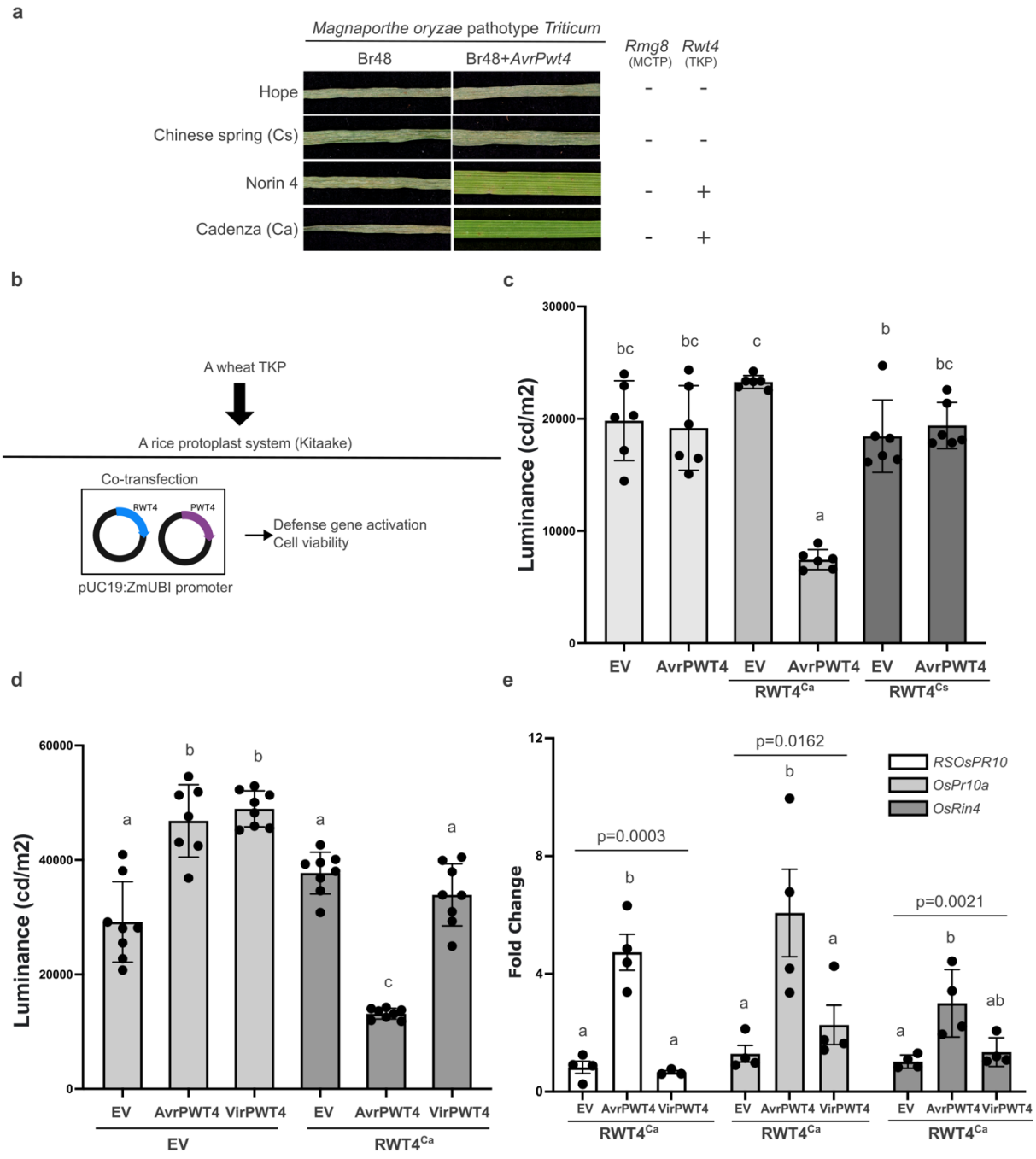


774

775 **Figure 1. RWT4-mediated resistance requires AvrPWT4 perception. (a)** Disease phenotyping of
776 wheat cultivars Hope, Chinese Spring (Cs), Norin 4, and Cadenza (Ca) with *Magnaporthe oryzae*
777 pathotype *Triticum* Br48 and a Br48 transformant carrying *AvrPwt4* (Br48+ *AvrPwt4*). Wheat
778 genotypes with (+) or without (-) functional *Rmg8* or *Rwt4* alleles are indicated. **(b)** Experimental
779 procedure of a rice protoplast transfection system for cell viability assays and defense gene

780 expression tests. Genes of interest (*Rwt4* or *Pwt4*) were cloned to a pUC19 vector containing a
781 maize polyubiquitin-1 (*Zm*Ubi-1) promoter. **(c)** RWT4 perceives AvrPWT4 triggering cell death
782 responses in rice protoplasts. RWT4 from Cadenza (Ca) and Chinese Spring (Cs) were assayed for
783 their perception of AvrPWT4 in rice protoplasts. Cell viability was measured as ATP activity
784 presented in luminance (cd/m$^2$). Luminescence (cd/m$^2$) was measured 16 h after protoplast
785 transfection. Six independent protoplast transfection events were used as biological replicates.
786 Mean±SEM are presented. Differences between treatments were analyzed using one-way ANOVA
787 with post-hoc Tukey HSD, $p<0.05$ **(d)** Only the recognized AvrPWT4 effector can induce RWT4$^{Ca}$-
788 triggered cell death. *Rwt4$^{Ca}$* was co-transfected with either the avirulent (*AvrPwt4*) or the virulent
789 (*VirPwt4*) allele of *Pwt4* in rice protoplasts. Protoplasts transfected with empty vector (EV) or co-
790 transfected with empty vector and *Pwt4* were treated as experimental controls. Experiments
791 were performed and analyzed as described in (c). **(e)** RWT4$^{Ca}$ recognition of AvrPWT4 activates
792 defense gene expression. Expression fold change of *RSOsPR10* (Os12g36830), *OsPr10a*
793 (Os12g36850) and *OsRin4* (Os04g0379600) defense genes were measured 7 h after protoplast
794 transfection. Gene expression was normalized to the internal control *OsUbq5* (Os01g22490), and
795 data were normalized to the samples transfected with *Rwt4$^{Ca}$*+EV as expression fold changes.
796 Mean±SEM from four transfection events is presented. Differences between treatments were
797 analyzed using one-way ANOVA with post-hoc Tukey HSD, $p<0.05$.
798
799
800
801

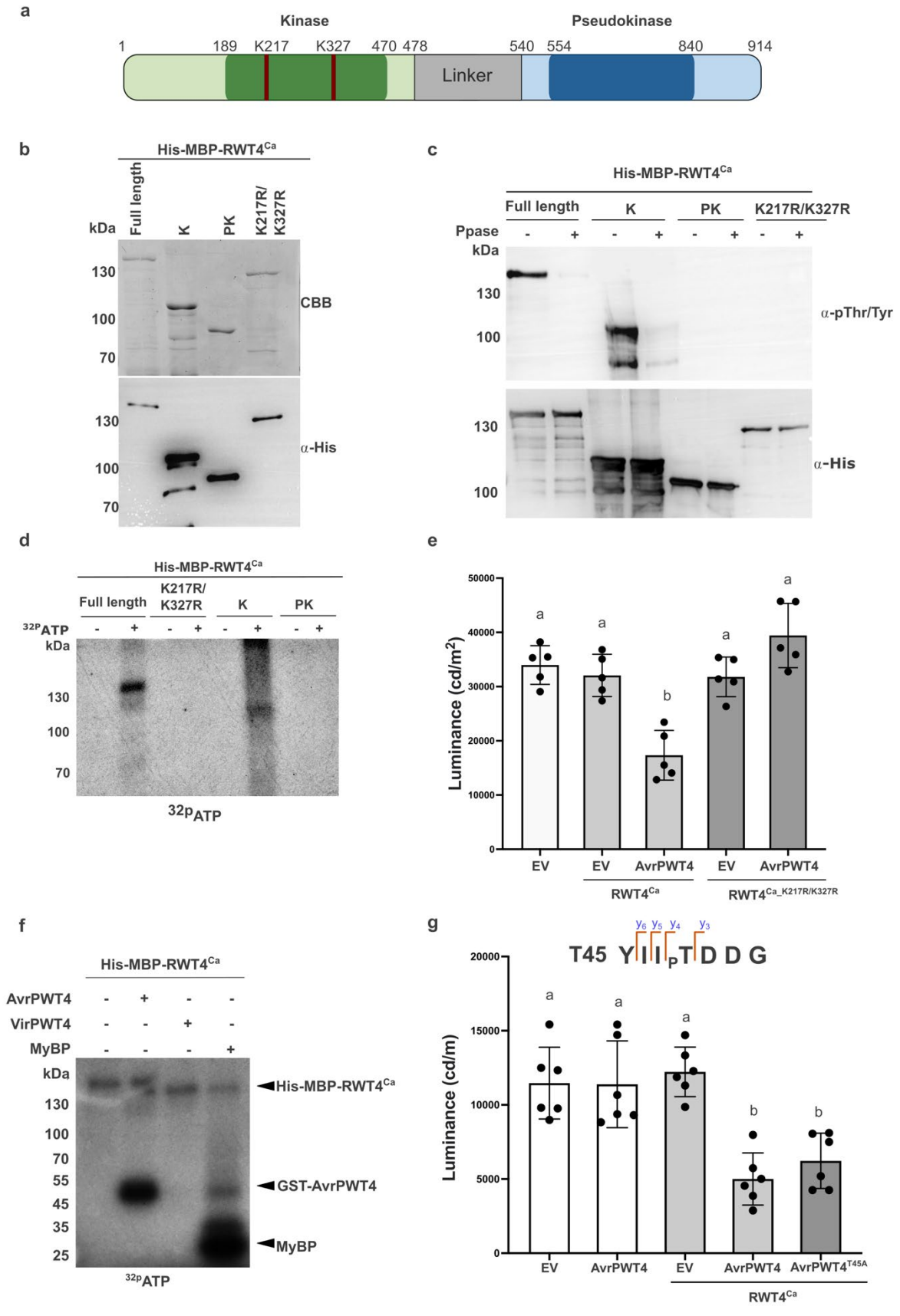
a
Kinase
Pseudokinase
1
189
K217
K327
470
478
540
554
840
914
Linker
b
His-MBP-RWT4Ca
Full length
K
PK
K217R/ K327R
kDa
130
100
70
CBB
α-His
c
His-MBP-RWT4Ca
Full length
K
PK
K217R/K327R
Ppase
kDa
α-pThr/Tyr
α-His
d
His-MBP-RWT4Ca
Full length
K217R/ K327R
K
PK
32PATP
kDa
32PATP
e
Luminance (cd/m2)
EV
EV
AvrPWT4
EV
AvrPWT4
RWT4Ca
RWT4Ca_K217R/K327R
f
His-MBP-RWT4Ca
AvrPWT4
VirPWT4
MyBP
kDa
His-MBP-RWT4Ca
GST-AvrPWT4
MyBP
32PATP
g
T45 YIIpTDDG
Luminance (cd/m)
EV
AvrPWT4
EV
AvrPWT4
AvrPWT4T45A
RWT4Ca

803 **Figure 2. RWT4 is an active kinase and transphosphorylates AvrPWT4. (a)** RWT4$^{Ca}$ encodes
804 kinase and pseudokinase architecture with a flexible linker between the two. The kinase and
805 pseudokinase domain borders are indicated in dark green and dark blue, respectively. Predicted
806 kinase active sites: K217 and K327. **(b)** Purity of recombinant proteins isolated from *E. coli.* His-
807 MBP-RWT4$^{Ca}$, kinase (His-MBP-K, amino acids 1-478), pseudokinase (His-MBP-PK, amino acids
808 540-914), and its kinase dead variant (RWT4$^{Ca_K217R/K327R}$) are shown by Coomassie brilliant blue
809 (CBB) stained SDS-PAGE and corresponding western blot using anti-His. **(c)** Autophosphorylation
810 activity of His-MBP-RWT4$^{Ca}$. Autophosphorylation status of the His-MBP-RWT4$^{Ca}$ proteins were
811 assayed by western blot using anti-phospho-Threonine/Tyrosine antibody (α-pThr/Tyr) with or
812 without lambda protein phosphatase incubation prior to separating by SDS-PAGE. Anti-His
813 western blotting (α-His) demonstrates equal loading of the His-MBP-RWT4$^{Ca}$ proteins. **(d)** Active
814 protein phosphorylation was measured by incubating the His-MBP-CaRWT4 proteins with [γ-
815 $^{32P}$]ATP before separating by SDS-PAGE and visualizing by autoradiography. **(e)** RWT4$^{Ca}$-AvrPWT4
816 triggered cell death requires RWT4$^{Ca}$ kinase activity. *Rwt4$^{Ca}$* and the kinase dead variant
817 (*Rwt4$^{Ca}$*$_{K217R/K327R}$) were co-transfected with *AvrPwt4* into rice protoplasts for cell viability assays.
818 Five independent protoplast transfection events were used as biological replicates and
819 Mean±SEM are presented. Treatment differences were analyzed using one-way ANOVA with post-
820 hoc Tukey HSD, $p<0.05$. **(f)** RWT4$^{Ca}$ specifically trans-phosphorylates AvrPWT4.
821 Transphosphorylation activity was assayed by mixing His-MBP-RWT4$^{Ca}$ and AvrPWT4 at room
822 temperature for 20 min before incubated with [γ-$^{32}$P]ATP. Phosphorylation of the substrate
823 proteins (AvrPWT4 or MyBP) were visualized via autoradiography. **(g)** Phosphorylated peptides
824 were mapped to the sequence of AvrPWT4 for functional analysis. The phosphorylated peptide
825 YIITDDG was identified from LC-MS/MS with the phosphorylation site T45. *Rwt4$^{Ca}$* was co-
826 transfected with either wild-type *AvrPwt4* or the phosphorylation null mutant *AvrPwt4$^{T45A}$* to rice
827 protoplasts. Luminescence (cd/m$^2$) was measured 16 h after protoplast transfection as an
828 indicator of cell viability. Six independent protoplast transfection events were used as biological
829 replicates. Mean±SEM are presented. Differences between treatments were analyzed using one-
830 way ANOVA with post-hoc Tukey HSD, $p<0.05$.
831

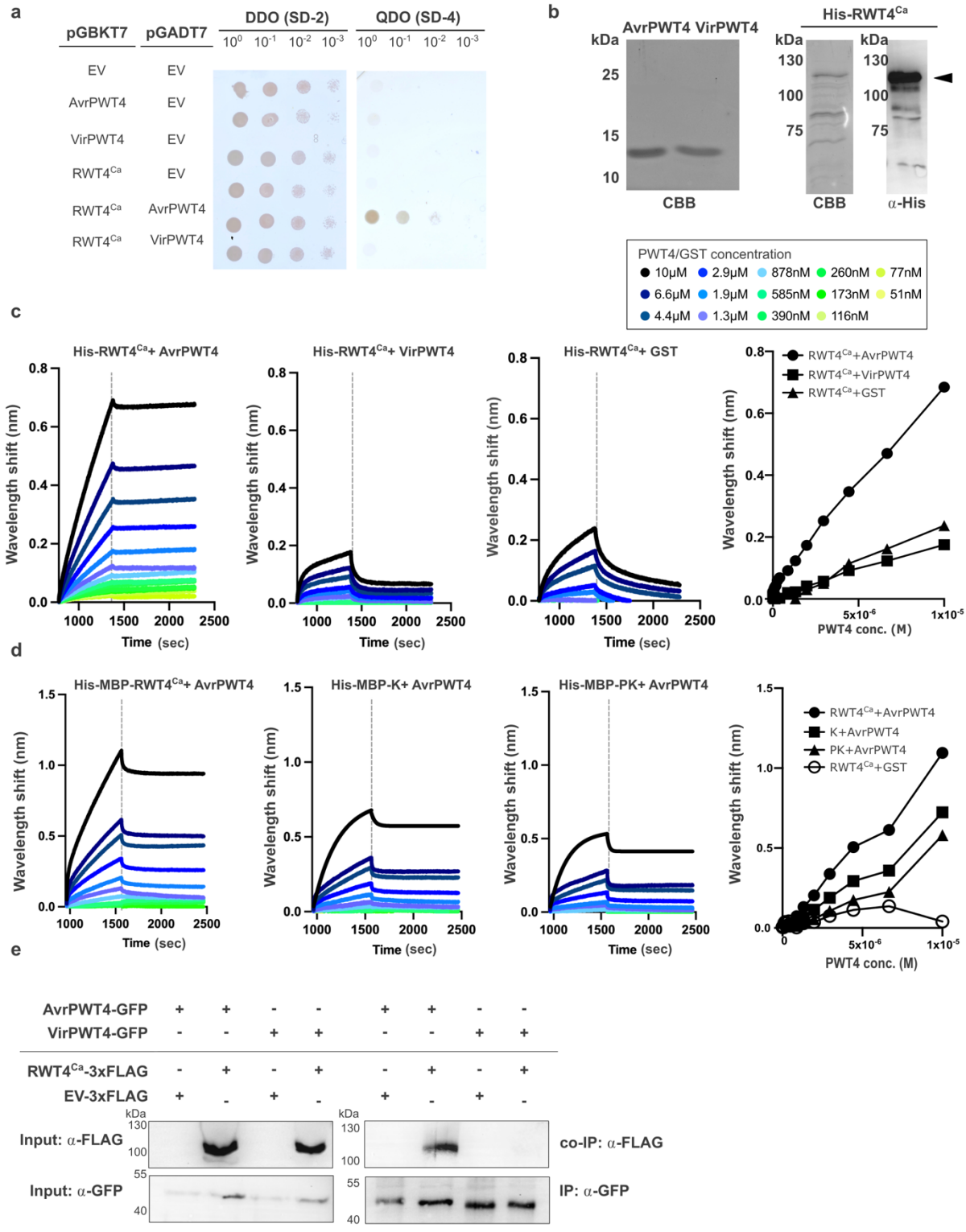
a
pGBKT7
pGADT7
DDO (SD-2)
QDO (SD-4)
EV
AvrPWT4
VirPWT4
RWT4Ca
b
AvrPWT4 VirPWT4
His-RWT4Ca
kDa
CBB
α-His
PWT4/GST concentration
10μM 2.9μM 878nM 260nM 77nM
6.6μM 1.9μM 585nM 173nM 51nM
4.4μM 1.3μM 390nM 116nM
c
His-RWT4Ca+ AvrPWT4
His-RWT4Ca+ VirPWT4
His-RWT4Ca+ GST
Wavelength shift (nm)
Time (sec)
PWT4 conc. (M)
d
His-MBP-RWT4Ca+ AvrPWT4
His-MBP-K+ AvrPWT4
His-MBP-PK+ AvrPWT4
K+AvrPWT4
PK+AvrPWT4
e
AvrPWT4-GFP
VirPWT4-GFP
RWT4Ca-3xFLAG
EV-3xFLAG
Input: α-FLAG
Input: α-GFP
co-IP: α-FLAG
IP: α-GFP

832

833 **Figure 3. RWT4$^{Ca}$ directly and specifically binds AvrPWT4. (a)** Yeast-two hybrid (Y2H) assays using
834 *Rwt4$^{Ca}$*, *AvrPwt4* and *VirPwt4*. *Rwt4$^{Ca}$* was cloned to the bait vector pGBKT7, while *AvrPwt4* and
835 *VirPwt4* were cloned into the prey vector pGADT7. Yeast growth on DDO (SD-Leu/-Trp) media
836 indicates the presence of the two plasmids, and the growth on QDO/X/A (SD-Ade/-His/-Leu/-
837 Trp/3-amino-1,2,4-triazole) media indicates interaction. Serial dilutions from cell suspensions of
838 a single yeast colony expressing the bait and prey plasmids are shown and represent the strength
839 of interaction. Empty vectors (EV) of pGBKT7 and pGADT7 were used as negative controls. **(b)**
840 Purity of AvrPWT4, VirPWT4, and His-RWT4$^{Ca}$. AvrPWT4 and VirPWT4 were expressed and
841 purified with a GST tag that was removed and separated by TEV protease and gel filtration. Purity
842 of His-CaRWT4 is shown by Coomassie brilliant blue (CBB) stained SDS-PAGE and Anti-His western
843 blotting (α-His). **(c)** and **(d)** Bio-layer interferometry (BLI) characterizes binding affinity between
844 His-RWT4$^{Ca}$ and PWT4 proteins. **(c)** His-RWT4$^{Ca}$ was mobilized to Ni-NTA biosensors as analytes
845 and incubated with a range of concentrations (51 nM to 10 µM) of AvrPWT4, VirPWT4, or GST
846 ligand proteins. Sensorgrams show BLI traces (wavelength shifts) during association and
847 dissociation steps (shown as time at the x-axis) normalized to no-ligand controls. The steady state
848 analysis (right) shows wavelength shifts against different ligand concentrations (AvrPWT4,
849 VirPWT4, or GST, from 10 µM to 116 nM). **(d)** His-MBP-RWT4$^{Ca}$, His-MBP-Kinase (K, amino acids
850 1-478) and His-MBP-Pseudokinase (PK, amino acids 540-914) proteins were immobilized to Ni-
851 NTA biosensors and incubated with AvrPWT4. Binding affinity between His-MBP-RWT4$^{Ca}$, His-
852 MBP-K and His-MBP-PK to AvrPWT4 were detected by BLI during association and dissociation
853 steps (shown as time at the x-axis) and presented in the steady state analysis against different
854 concentrations of AvrPWT4 (right). **(e)** *In-planta* interaction of RWT4$^{Ca}$ and AvrPWT4. AvrPWT4-
855 GFP or VirPWT4-GFP were co-expressed with RWT4$^{Ca}$-3xFLAG in *N. benthamiana* using
856 *Agrobacterium*-mediated transient expression and subjected to anti-GFP immunoprecipitation
857 (IP). Input and IP samples were immunoblotted with anti-FLAG and anti-GFP antibodies.
858

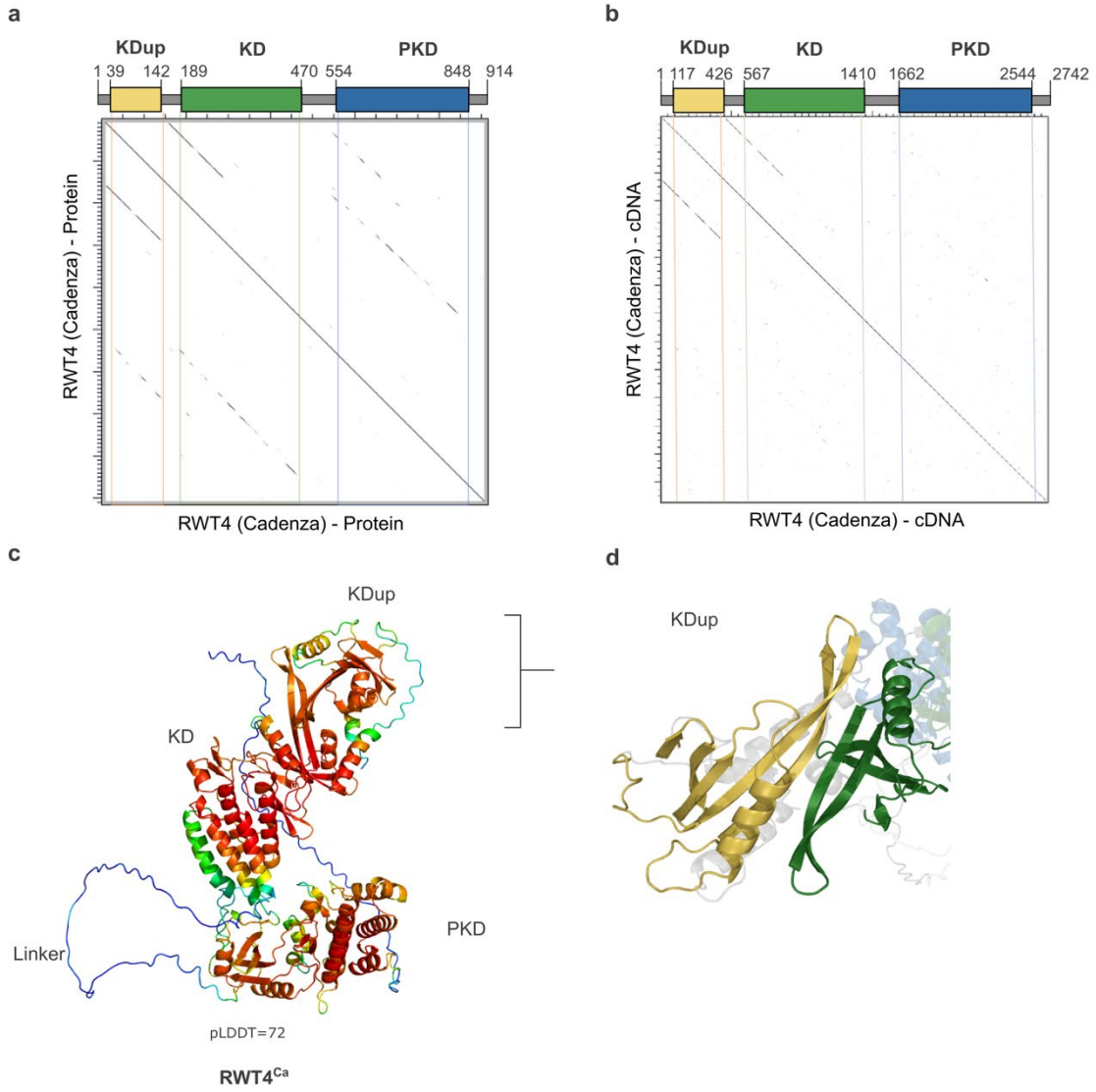


**Figure 4. The kinase region of RWT4$^{Ca}$ contains an integrated N-terminal truncated kinase duplication (KDup). (a)** Dot plot of the RWT4$^{Ca}$ protein demonstrating collinearity between KDup (amino acids 39-142) and a segment of the kinase domain in amino acids 150-290. KD = kinase domain, PKD = pseudokinase domain. Vertical lines denote domain borders, diagonal lines indicate collinearity. **(b)** Dot plot of the *RWT4$^{Ca}$* cDNA demonstrating collinearity between KDup and a segment of the kinase domain (88.73% identity). **(c)** AlphaFold model of RWT4$^{Ca}$, colored by pLDDT score. **(d)** Structural similarity between the KDup (yellow) and KD (green).

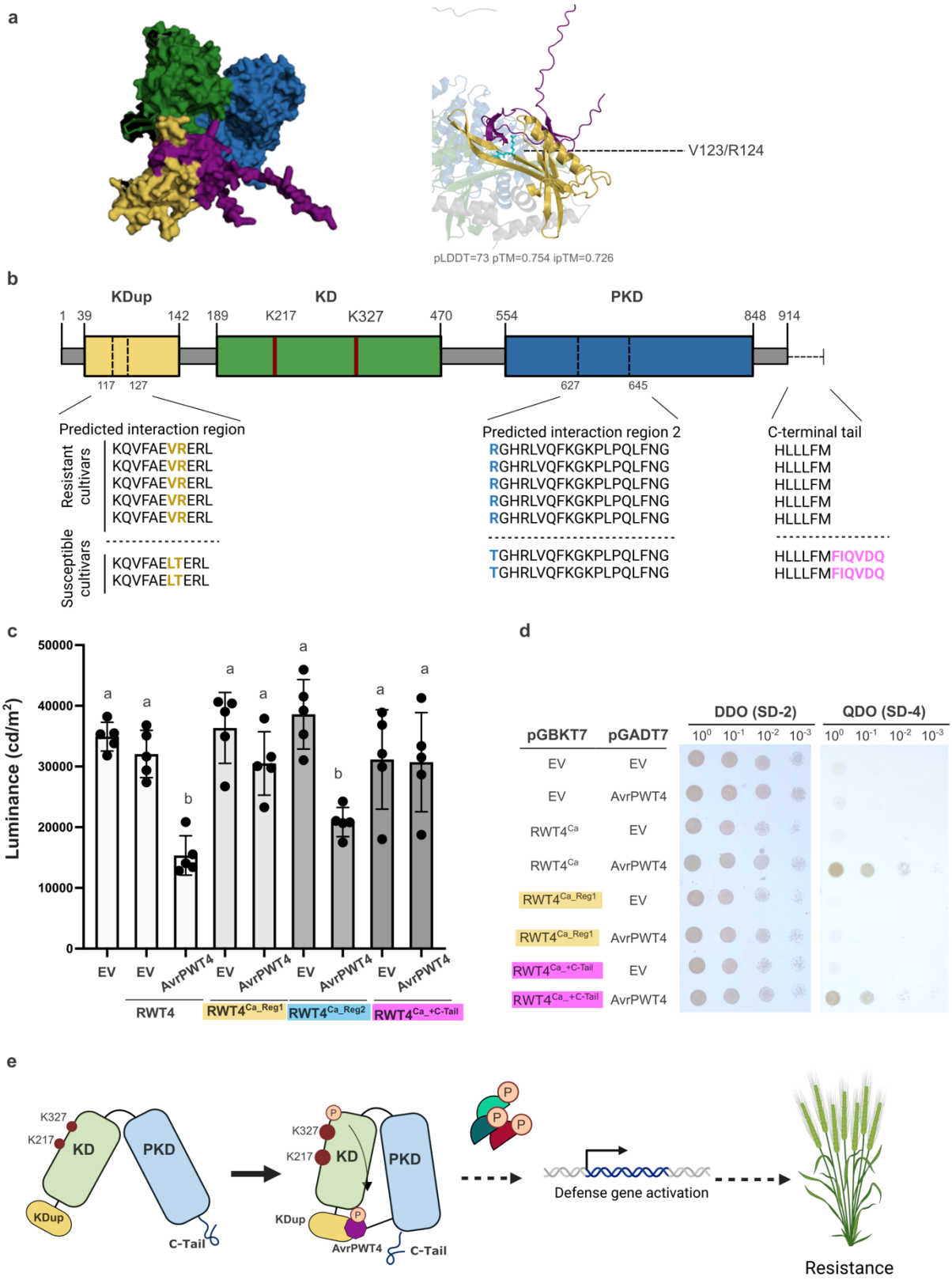
a
V123/R124
pLDDT=73 pTM=0.754 ipTM=0.726
b
KDup
KD
PKD
1 39 142 189 K217 K327 470 554 848 914
117 127 627 645
Predicted interaction region
Resistant cultivars
KQVFAEVRERL
KQVFAEVRERL
KQVFAEVRERL
KQVFAEVRERL
KQVFAEVRERL
Susceptible cultivars
KQVFAELTERL
KQVFAELTERL
Predicted interaction region 2
RGHRLVQFKGKPLPQLFNG
RGHRLVQFKGKPLPQLFNG
RGHRLVQFKGKPLPQLFNG
RGHRLVQFKGKPLPQLFNG
RGHRLVQFKGKPLPQLFNG
TGHRLVQFKGKPLPQLFNG
TGHRLVQFKGKPLPQLFNG
C-terminal tail
HLLLFM
HLLLFM
HLLLFM
HLLLFM
HLLLFM
HLLLFMFIQVDQ
HLLLFMFIQVDQ
c
Luminance (cd/m2)
50000
40000
30000
20000
10000
0
a a b a a a b a a
EV EV AvrPWT4 EV AvrPWT4 EV AvrPWT4 EV AvrPWT4
RWT4
RWT4Ca_Reg1
RWT4Ca_Reg2
RWT4Ca_+C-Tail
d
pGBKT7
pGADT7
DDO (SD-2)
QDO (SD-4)
10^0 10^-1 10^-2 10^-3
EV EV
EV AvrPWT4
RWT4Ca EV
RWT4Ca AvrPWT4
RWT4Ca_Reg1 EV
RWT4Ca_Reg1 AvrPWT4
RWT4Ca_+C-Tail EV
RWT4Ca_+C-Tail AvrPWT4
e
K327
K217
KD
PKD
KDup
C-Tail
P
AvrPWT4
Defense gene activation
Resistance

868

869 **Figure 5. Structure-guided identification of RWT4 specificity. (a)** AlphaFold Multimer modeling
870 predicts that AvrPWT4 (purple) forms an interaction complex between the integrated kinase
871 duplication (KDup, yellow) and pseudokinase (blue). The predicted binding region V123/R124 in
872 RWT4's KDup is highlighted (cyan, right panel). pLDDT indicates confidence in structure modeling
873 and pTM and ipTM indicate the confidence for interaction. The kinase (green, 1-470) and
874 pseudokinase (554-914) regions were separately inputted for modeling, with the linker region
875 removed. **(b)** Illustration of sequence and structure features of RWT4$^{Ca}$. *Rwt4* sequences were
876 obtained from resistant wheat cultivars (Norin 4, Cadenza, Jagger, Paragon, and Claire) and
877 susceptible wheat cultivars (Chinese Spring and CDC Stanley). Kinase active sites are indicated in
878 red. The interaction regions were identified based on the modeling from (**a**). **(c)** RWT4$^{Ca}$ variants
879 validate the requirement of Region 1 and C-terminal sequences for defense activation. *Rwt4$^{Ca}$*
880 and its variants (*Rwt4*$^{Ca_Reg1}$: V123L/R124T, *Rwt4*$^{Ca_Reg2}$: R627T, *Rwt4*$^{Ca_+C\text{-}Tail}$: RWT4$^{Ca}$ with the
881 extended C-terminal residues FIQVDQ) were co-transfected with *AvrPwt4* into rice protoplasts.
882 Cell viability was measured as ATP activity presented in luminance (cd/m$^2$). Data are represented
883 as the mean ± SEM (n= 5). Different letters indicate significant differences using one-way ANOVA
884 with post-hoc Tukey HSD ($P \leq 0.05$). **(d)** Yeast-two hybrid confirms the interaction between
885 RWT4$^{Ca}$ variants to AvrPWT4. *Rwt4$^{Ca}$* and its variants *Rwt4*$^{Ca_Reg1}$, and *Rwt4*$^{Ca_+C\text{-}Tail}$ were cloned to
886 the bait vector pGBKT7 while *AvrPwt4* was cloned to the prey vector pGADT7. The transformation
887 of bait and prey vectors were confirmed by yeast growth on DDO (SD-Leu/-Trp) media. The
888 interaction was assayed by growth on QDO (SD-Ade/-His/-Leu/-Trp/3-amino-1,2,4-triazole) media.
889 Serial dilutions from cell suspensions of a single yeast colony expressing the bait and prey
890 plasmids are shown and represent the strength of interaction. Empty vectors (EV) of pGBKT7 and
891 pGADT7 were used as negative controls. **(e)** RWT4 working model. KD = kinase domain, PKD =
892 pseudokinase domain, KDup = integrated kinase duplication, P = phosphorylation, red = RWT4$^{Ca}$
893 kinase active sites, C-Tail = C-terminal tail of RWT4.
894
895
896
897